

Article

# Comparative Analysis of the Effect of Cutting Piezoelectric Ceramics on Optically Oriented Compensation Capability

Bo Li <sup>1,2</sup> and Dapeng Tian <sup>1,2,\*</sup> 

<sup>1</sup> The Key Laboratory of Airborne Optical Imaging and Measurement, Changchun Institute of Optics, Fine Mechanics and Physics, Chinese Academy of Sciences, Changchun 130033, China; libo221@mailsucas.ac.cn

<sup>2</sup> University of Chinese Academy of Sciences, Beijing 100049, China

\* Correspondence: d.tian@ciomp.ac.cn

**Abstract:** In a photoelectric tracking system, a deformable mirror can be used to adjust the transmission path of a light beam to achieve accurate measurement and tracking of the target position. The single-piezoelectric-sheet deformable mirror is a commonly used wavefront correction device with outstanding advantages, such as its simple structure, low cost, and easy preparation. However, it usually has a large cross-linking value and a weak ability to correct higher-order wavefront aberrations. To solve this problem, a novel single-piezoelectric-sheet deformable mirror driving structure is proposed in this paper, in which the coupling between the driving units is weakened by laser cutting the piezoelectric ceramics along the electrode gaps to reduce the cross-linking value of the deformable mirror. In order to verify the effectiveness of this driving structure, this paper takes the 85-unit single-piezoelectric-sheet deformable mirror as an example and simulates the influence function for different cutting depth conditions. The simulation results show that the cross-linking value between neighboring drive units decreases significantly as the piezoelectric-ceramic-laser cutting depth of the drive electrode gap increases. When the piezoelectric ceramic was laser cut to a depth of half of the overall thickness, the cross-linking value decreased by 6.8%.

**Keywords:** piezoelectric deformable mirror; adaptive optics; cross-linking value; photoelectric imaging



**Citation:** Li, B.; Tian, D. Comparative Analysis of the Effect of Cutting Piezoelectric Ceramics on Optically Oriented Compensation Capability. *Photonics* **2023**, *10*, 1136. <https://doi.org/10.3390/photonics10101136>

Received: 7 September 2023

Revised: 8 October 2023

Accepted: 9 October 2023

Published: 11 October 2023



**Copyright:** © 2023 by the authors. Licensee MDPI, Basel, Switzerland. This article is an open access article distributed under the terms and conditions of the Creative Commons Attribution (CC BY) license (<https://creativecommons.org/licenses/by/4.0/>).

## 1. Introduction

The photoelectric tracking system is a technology based on optical technology to achieve the function of the target tracking and positioning system, which usually includes cameras and photoelectric sensors to monitor the position and motion information of target objects [1]. It is widely used in aerospace, navigation, military, and robotics. Photoelectric tracking systems can obtain real-time information about the motion of the target and control it as needed in order to achieve accurate tracking and positioning of the target. In some cases, photoelectric tracking systems need to correct wavefront aberrations in the optical system in order to achieve the system to maintain high-precision tracking of the target [2].

Adaptive optics is a technique applied to optical systems to correct aberrations by adjusting the shape or characteristics of optical elements in real time to obtain better image quality. This technique was initially developed to solve the aberration problem in ground-based telescopes under the influence of atmospheric turbulence [3]. Adaptive optics systems utilize sensors to monitor the propagation of light waves in real time and correct these aberrations with controllers and compensation devices. Deformable mirrors were first proposed to solve the problem of aberrations in ground-based telescopes under the effect of atmospheric turbulence. As one of the core devices of adaptive optics systems, it has good application prospects in both military and civilian fields, and optimizing its parameter design has a crucial impact on the overall performance [4,5]. Atmospheric turbulence can lead to phase differences in the incident light wavefront, thus reducing the resolution and imaging quality of the telescope. By adding a deformable mirror to the

optical system of the telescope, the shape of the mirrors can be adjusted in real time to offset the phase difference caused by atmospheric turbulence, thus improving the observing capability of the telescope [6]. According to the different working principles and materials, deformable mirrors can be categorized into various types, such as electrostatic-driven [7], electromagnetic-driven [8], and piezoelectric-driven [9]. Among these, the piezoelectric deformable mirror is a common type. It utilizes the piezoelectric effect, in which certain crystals change shape under the action of an electric field. It makes use of the piezoelectric effect, which usually has the advantages of a compact and lightweight structure, fast response speed, high deformation accuracy, and wide application band [10].

The piezoelectric deformable mirror is made of piezoelectric crystal material, and the curvature and shape of the mirror are adjusted by applying a voltage to change the shape of the crystal [11,12]. The piezoelectric deformable mirror has significant advantages over other types of mirrors [13]. First of all, it has a fast response speed, which can quickly respond to external excitation and achieve high-speed shape adjustment, suitable for fast optical systems. Secondly, it has high shape adjustment accuracy, which can achieve sub-nanometer deformation and is suitable for high-precision optical systems. Thirdly, its power consumption is low; a piezoelectric deformable mirror only needs to apply a very small voltage when working, so its power consumption is relatively low [14]. Fourthly, it is highly reliable, with a simple, lightweight structure and no internal mechanical parts or wearing parts. Finally, the precision of piezoelectric deformable mirrors can reach sub-micron level, which is finer than other principle mirrors. Moreover, due to the special nature of the piezoelectric effect, piezoelectric deformable mirrors can realize a wide range of surface deformations, which can satisfy the demand of adjusting different wavelengths [15]. However, there are some drawbacks; the displacement range of piezoelectric deformable mirrors is small and not suitable for large displacement applications. The performance of piezoelectric materials is greatly affected by temperature [16]. Its working temperature range is strict, and the mechanical and electrical properties of piezoelectric materials change at different temperatures, causing instability, so temperature compensation is needed [17]. The larger cross-linking values are due to the fact that the piezoelectric deformable mirrors are designed to obtain higher mechanical strength and stability and to improve the rigidity and stability of the material. The structural design of the piezoelectric ceramics has not been updated, resulting in larger cross-linking values for piezoelectric deformable mirrors compared to other types, which is reflected in this paper.

Based on the content of our knowledge, other studies usually only consider the effect of the overall thickness of the piezoelectric ceramic, the shape of the electrodes, the way the electrodes are arranged, and the way the edges are supported on the deformable mirror performance [18–20]. Ningbo University prepared a 19-unit 50 mm caliber deformable mirror prototype in [21]. A two-wafer deformable mirror with 20 electrodes on a 63 mm aperture was designed in reference [22]. Piezoelectric-stack deformable mirrors with 61 piezoelectric actuators and a 60 mm aperture and dual-wafer deformable mirrors with 48 electrodes and a 50 mm aperture have been established in reference [23]. To this end, a simple and low-cost 85-unit silicon-based single-piezoelectric-sheet deformable mirror is proposed in this paper, in which the processed thickness of the piezoelectric ceramic is adjusted by laser cutting, and the electrode shape is ensured to remain unchanged. The processing of the thickness does not exceed 50% of the piezoelectric material's thickness (Laser cutting the PZT sheet deeper than 50% caused serious carbonation and made the actuators fragile.). The deflection and cross-linking value of the deformable mirror are taken as two indicators affecting the calibration performance.

Later in this paper, there is a significant decrease in the cross-link value when cutting the non-electrode region of the piezoelectric material. This is due to the fact that the cutting process destroys the structure of the piezoelectric ceramic material and reduces its cross-linking properties. It is possible to add degrees of freedom to the single-piezoelectric-sheet deformable mirror to achieve a faster deformation speed; reduce the inertia effect, making the response faster and better adapted to external changes; reduce the thickness of the

piezoceramics by cutting, which reduces the size and the weight; and reduce the thickness of the piezoceramics to increase their intrinsic frequency, thus improving the frequency response range of the deformable mirror.

The remainder of this article is organized as follows. Section 2 describes the background, underlying theory, and modeling of piezoelectric deformable mirrors. Section 3 introduces and presents the analysis of the proposed method in this study. Section 4 describes the analysis of the simulation results of the proposed method. Finally, Section 5 concludes this article.

## 2. Background and Modeling of Piezoelectric Deformable Mirrors

This section introduces background on piezoelectric deformable mirrors and their modeling. It also describes some basic concepts of piezoelectric deformable mirrors, such as influence functions and cross-linking values.

### 2.1. Piezoelectric Materials and the Piezoelectric Effect

The piezoelectric material chosen for the piezoelectric deformable mirror designed in this article is PZT-5H. PZT-5H is a commonly used lead zirconate titanate (PZT) ceramic material with good piezoelectric properties. It has a high piezoelectric coefficient and piezoelectric stress constant, which can produce a large deformation response when an electric field is applied. It also has high mechanical strength and toughness to withstand large stresses and strains, resulting in better stability and durability during deformable mirror operation.

The piezoelectric effect refers to the fact that when an external force is applied to the surface of a piezoelectric material, the material separates the positive and negative charges, resulting in an imbalance in the internal distribution of charges, which leads to the formation of potential differences and voltages [24]. The schematic diagram is shown in Figure 1a. The inverse piezoelectric effect is the inverse process of the positive piezoelectric effect. When an external electric field is applied to a piezoelectric material, the material deforms, resulting in mechanical stress. The schematic diagram is shown in Figure 1b. PDM utilizes the inverse piezoelectric effect, whereby an applied electric field creates mechanical stress through the piezoelectric material, which facilitates the displacement of the mirror.

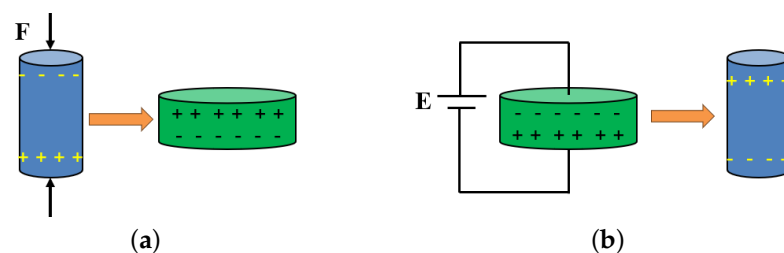


**Figure 1.** Piezoelectric effect schematic diagram: (a) Piezoelectric effect schematic diagram. (b) Inverse piezoelectric effect schematic.

### 2.2. Piezoelectric Deformable Mirror Structure

The initial model of the 85-unit PDM is shown in Figure 2a and consists of a 500  $\mu\text{m}$  thick layer of monocrystalline silicon material and a 300  $\mu\text{m}$  thick layer of the piezoelectric material—lead zirconate titanate (PZT-5H)—with a silver-coated layer on the surface of the optics, which is generally in the range from about 80 nm to 150 nm in thickness.

The diameter of the deformable mirror is 50 cm, and the effective calibrated aperture is 46 cm. In this paper, we investigate the effect of different thicknesses of the piezoelectric layer on the optical system. The inner surface of the piezoelectric layer is covered with a metal film as a common electrode, while the outer surface is covered with a patterned array of electrodes. The operating voltage range was  $-150\sim+150$  V. We kept the thickness of the electrode region constant and cut the non-electrode region by laser cutting and

other methods. In addition, we coated the outer surface of the wafer with a metallic or dielectric reflective layer. We chose monocrystalline silicon material for the deformable mirrors' optical mirror compared to conventional glass materials because of its excellent mechanical properties, compatibility with micromachining processes, and the easy availability and low cost of commercially polished silicon wafers. These wafers can achieve thicknesses of 200~1000  $\mu\text{m}$  and diameters of 50~100 mm, and the polished surfaces have good optical properties.

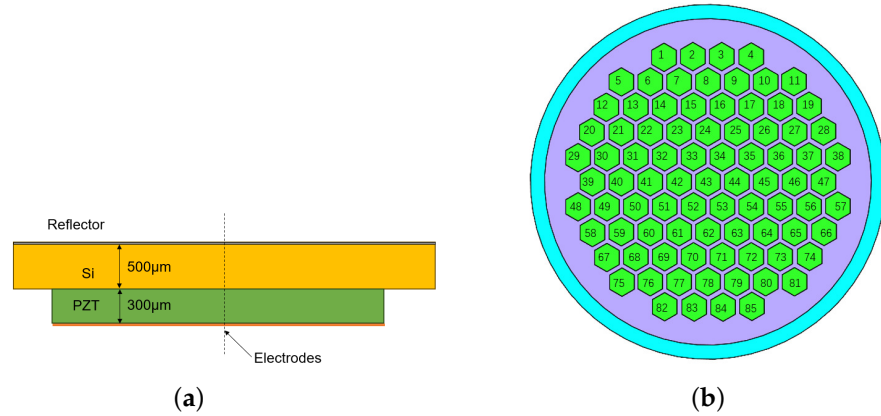


**Figure 2.** Schematic diagram of 85-unit piezoelectric deformable mirror. (a) Cross-sectional view of deformable mirror. (b) Distribution of the 85 electrodes.

2.3. Cross-Linking Value

Cross-linking value is a parameter of the strength and stiffness of the surface of a deformable mirror. It describes the properties of the deformable mirror material, including its stiffness, elasticity, and deformability [25]. The driver cross-linking value, which is the ratio of the deformation  $\delta$  of the energized driver in a single influence function to the deformation  $\delta$  of the drivers in adjacent positions. The detailed schematic, shown in Figure 3, is as follows

$$\omega = \frac{\delta_2}{\delta_1} \tag{1}$$

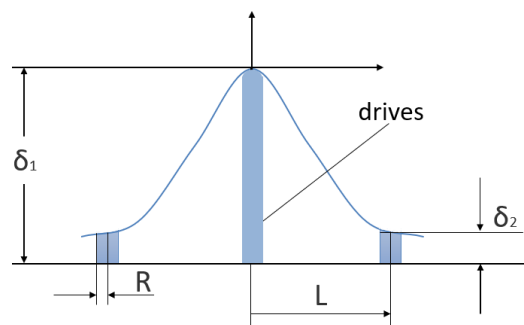


**Figure 3.** Figure of the method for calculating the cross-linking values of deformable mirrors.

The larger the change in cross-linking value, the smoother the wavefront change, and the smaller the cross-linking value, the steeper the wavefront change. Different cross-linking values can also seriously affect the ability of the deformable mirror to correct the phase of the wavefront. The definitions and calculations of the cross-linking value in this article are described later.

3. Design of Electrode Gap Cutting for Piezoelectric Deformable Mirrors

This section focuses on how to select the ortho-hexagonal pattern among several common piezoelectric deformable mirror electrode patterns, the design of the cutting

region, and the method of calculating the cross-linking value based on the piezoelectric deformable mirror structures covered in this paper.

### 3.1. Design of Electrode Pattern and Selection of Cutting Area

The dominant electrode patterns today are square hexagons or circles. Comparisons have shown that more actuators can be mounted on a hexagonal electrode than on a circular electrode for the same area with the same diameter of mirror or piezoelectric ceramic material. Figure 4 illustrates this point. The individual hexagonal electrodes in (a,b) have the same area as the circular electrodes, but 85 are arranged in (a), while only 69 are arranged in (b). Additionally, the piezoelectric material has the same area, so (a) has a higher fill ratio than (b), which is more valuable in practical applications.

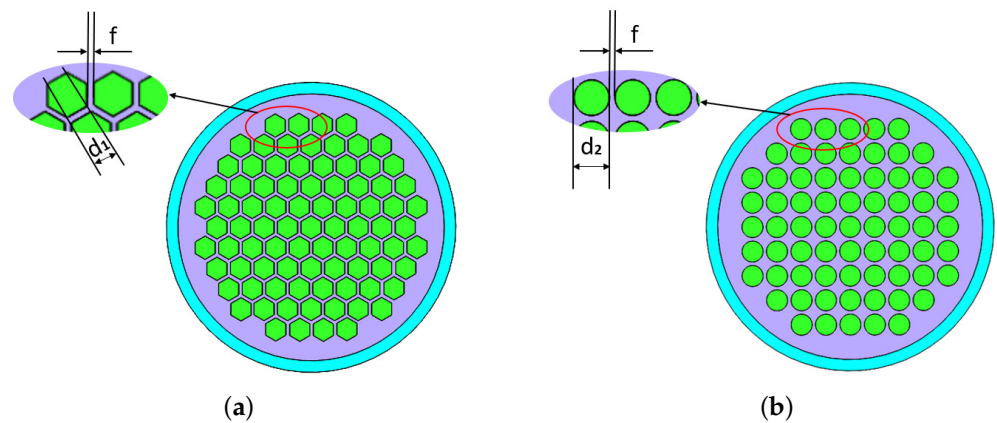


**Figure 4.** Figures describing deformable mirrors with different electrode shapes. (a) Distribution of electrode shapes in an ortho-hexagonal shape. (b) Circular electrode shape distribution diagram.  $d_1 = 2$  mm,  $d_2 = 3.638$  mm,  $f = 0.69$  mm.

As shown in Figure 4, at equal actuator areas and electrode spacing, our piezoelectric deformable mirror with circular mirror aperture can accommodate 85 hexagonal actuators in a hexagonal lattice (Figure 4a) but only 69 circular actuators in a square lattice (Figure 4b). We chose the hexagonal arrangement because it provides a dense actuator placement and achieves a high fill ratio.

$$3 \times \sin \frac{\pi}{3} \times d_1^2 = \pi \left( \frac{d_2}{2} \right)^2 \tag{2}$$

An increase in the number of actuators is beneficial to the performance of a piezoelectric deformable mirror. It provides a greater deformation range, higher resolution, and faster response. Therefore, electrodes with regular hexagonal shapes are used in this study.

In other studies exploring the effect of the thickness of piezoelectric deformable mirrors on their performance, usually, only the thickness of the whole electrode has been considered for the study. In contrast, in this paper, a more innovative cutting region is considered, where the piezoelectric ceramic material is cut at different depths except for the electrode region, such as the purple area in Figure 4a.

In order to investigate the effect of the cutting depth of the piezoelectric ceramic electrode gap region on the performance of the piezoelectric deformable mirror, four groups of programs were designed, as shown in Figure 5. The cutting depths of the cut electrode gap region were 0  $\mu\text{m}$ , 37.5  $\mu\text{m}$ , 75  $\mu\text{m}$ , and 150  $\mu\text{m}$ , respectively (12.5%, 25%, and 50% of the total thickness of 300  $\mu\text{m}$ ). The deformable mirror’s deformable ability changes were observed by designing different depths of cut.

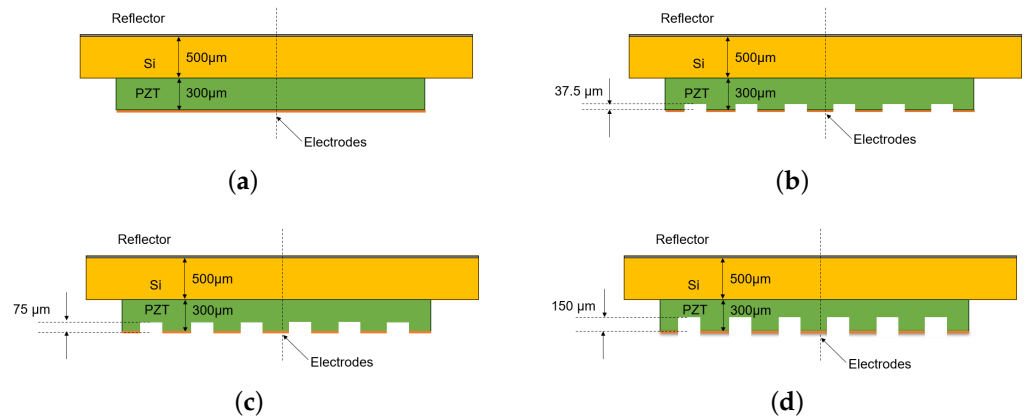


**Figure 5.** Schematic diagram of cutting depth: (a) 0  $\mu\text{m}$  depth of cut; (b) 37.5  $\mu\text{m}$  depth of cut; (c) 75  $\mu\text{m}$  depth of cut; (d) 150  $\mu\text{m}$  depth of cut.

3.2. Proposed Method of Calculating the Cross-Linking Value for This Structure

For the structure of the 85-unit piezoelectric deformable mirror proposed in this paper, a method for calculating the cross-linking value is proposed. If the electrode sheet used to calculate the cross-linking value is located at the edge, the displacements of the center points of several electrode regions nearest to its center point are added and averaged. If the electrode sheet for calculating the cross-linking value is not located at the edge, the calculation parameters are taken from the several electrode regions closest to its center point, which is usually six drivers in this structure. As shown in Figure 6, when analyzing electrode No. 43, which is located at the center, we need to consider electrodes No. 33, 34, 42, 44, 52, and 53, which are at the closest distance around it. When analyzing electrode 1 at the edge, we only need to consider electrodes No. 2, 6, and 7 because they are the only three electrodes within the closest distance. This is calculated by averaging the displacements of electrodes No. 33, 34, 42, 44, 52, and 53 and comparing them with the displacement of electrode No. 43. The displacements of electrodes No. 2, 6, and 7 are averaged and compared with the displacement of electrode No. 1.

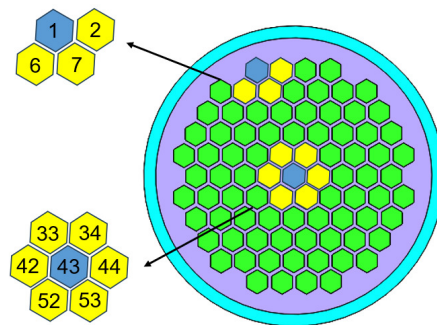


**Figure 6.** Figure of illustration of the calculation of the cross-linking values of this structure.

3.3. Simulation Parameter Setting

The designed 85-unit piezoelectric deformable mirror structure was imported into finite-element simulation software. In this study, 50 V was applied individually and separately in the order of electrode numbering, and fixed constraints were applied to the mirror edges. The mechanical restriction tooling for the free actuator electrodes is shown in Figure 7. The base is not included in the simulation and the perimeter of the piezoelectric sheet deformation mirror is glued to the tooling with epoxy adhesive. When the piezoelectric sheet is energized, there is no effect on the deformation of the tooling.

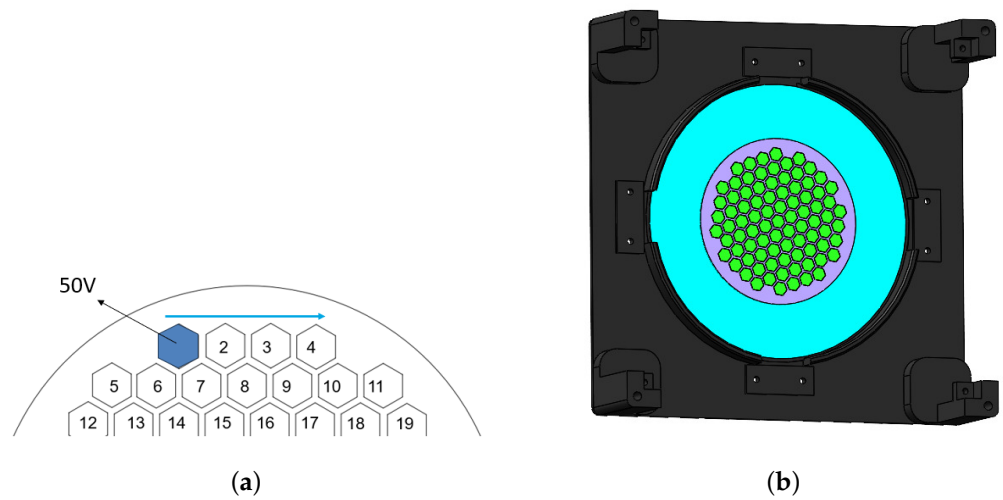


**Figure 7.** Figure of a description of the condition setting for piezoelectric deformable mirrors in the simulation. (a) Schematic diagram of the sequence of applying 50 V to the electrodes. (b) Schematic diagram for applying fixed constraints to mirror edges.

The piezoelectric deformable mirror is modeled using finite-element simulation software, applying electrostatic field and solid mechanics to establish the relationship between the stated voltage and the amount of deformation through the piezoelectric effect. In the finite-element model, the diameter and thickness of the mirror are set to be 50 cm and 500  $\mu\text{m}$ , respectively; the diameter of the piezoelectric material is 46 cm, the thickness of the piezoelectric material is 300  $\mu\text{m}$ , the electrode material is silver with a thickness of about 1–3  $\mu\text{m}$ , and a free tetrahedral mesh is delineated for the overall structure. The material parameters of the piezoelectric deformable mirror are shown in Table 1:

**Table 1.** Deformable mirror material parameters.

	Unit	Si	PZT-5H	Ag
Young’s modulus	[E/GPa]	170	68	83
Poisson’s ratio	[ $\nu$ ]	0.28	0.3	0.37
Piezoelectric coefficient	[ $d_{31}/(\text{pm}\cdot\text{V}^{-1})$ ]	-	-450	-

#### 4. Results

This section shows the results of applying various different constraints to the piezoelectric deformable mirror and simulating it in finite-element software. It contains the amount of mirror deformation, the influence function curve, the cross-linking value, and the linearity index between input and output.

First, we place a fixed constraint on the edge of the mirror and then apply 50 V to all electrodes simultaneously. The displacement results are shown in Figure 8. It can be seen that at any cutting depth, the maximum value of the entire mirror displacement is located in the most central area of the mirror. This is due to the fixed constraint we place on the specular edge, so the position variant closer to the edge is smaller. From the overall point of view, the maximum deformation of the mirror gradually decreases as the cutting depth deepens. This phenomenon occurs because the volume of the piezoelectric material decreases, and the charge generated by the inverse piezoelectric effect decreases.

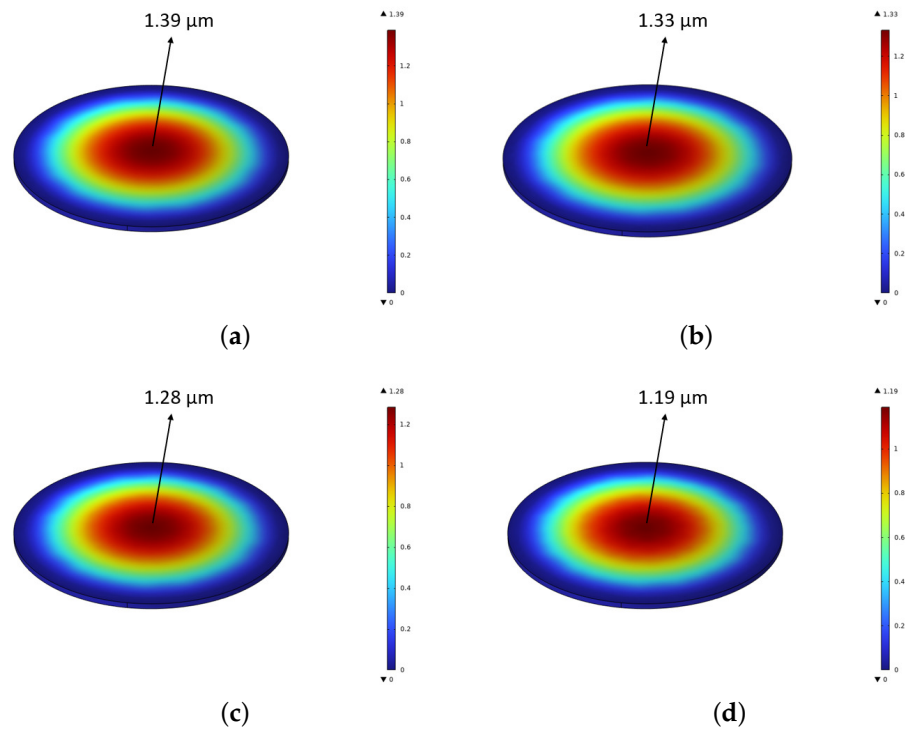


**Figure 8.** Figures of simulated deformation of all electrodes electrified with 50 V simulated deformable mirror. (a) Figure is the simulation of deformable mirror shape variable of 0  $\mu\text{m}$  depth of cut. (b) Figure is the simulation of deformable mirror shape variable of 37.5  $\mu\text{m}$  depth of cut. (c) Figure is the simulation of deformable mirror shape variable of 75  $\mu\text{m}$  depth of cut. (d) Figure is the simulation of deformable mirror shape variable of 150  $\mu\text{m}$  depth of cut.

We applied a voltage value of 50 V to each of the individual electrodes by applying them in the order of the electrode serial number and taking the center point of each positive hexagonal electrode as the coordinates for counting the displacement. Using the mirror surface as the zero reference surface, the resulting histogram of the shape variable of each electrode region is obtained, as shown in Figure 9.

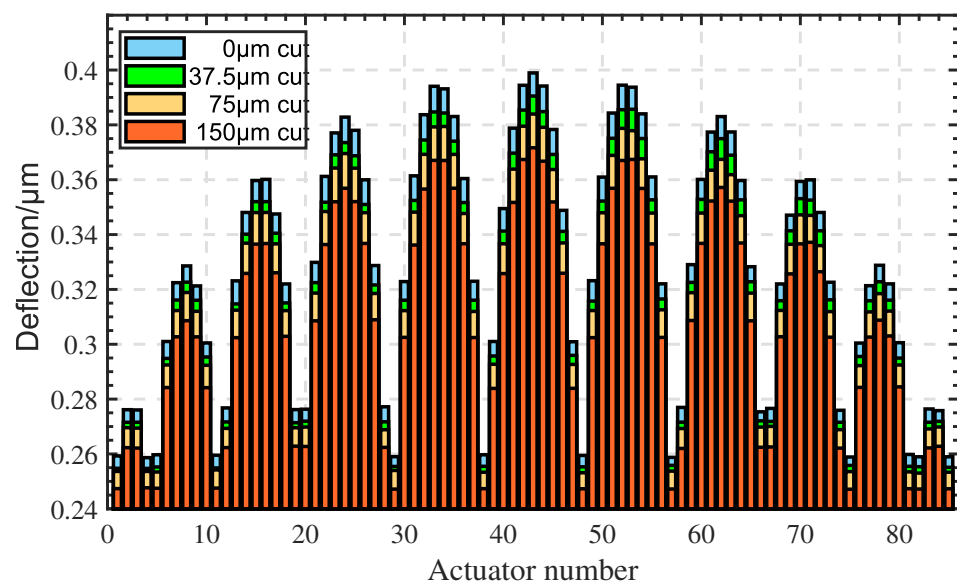


**Figure 9.** Figure of the amount of deformation produced at the center of a single electrode when a voltage of 50 V is applied to that electrode, with the actuator number in the horizontal coordinate and the amount of deflection in the vertical coordinate.

The overall graph of deflection shows a sinusoidal-like function curve, with the overall trend increasing the closer we become to electrode 43. The reason for this phenomenon is that the closer electrode No. 43 is, the closer its position on the piezoelectric material is to the center, and the less the effect of the edge fixation constraint is applied. In the process of converging to electrode No. 43, there will also be the image of a small sinusoidal wave. For examples, see No. 0–4, No. 5–11, No. 12–19. . . . The reason is the same as above: there is a significant decrease in the deflection at the position close to the edge.

In the structural design of the piezoelectric deformable mirror, the electrodes are placed in a circular array. Therefore, when plotting the influence function curves to infer the wavefront characteristics of the entire surface shape, we selected five electrodes on the circumferential diameter. However, electrode No. 47 is close to the edge, and, within the deformable mirror with a small diameter, the error is large, so it is rounded off. The remaining four electrodes can be used as representatives of the rest of the electrodes, and, with them, the wavefront phase of the whole mirror can be fitted by a specific algorithm. So, No. 43, 44, 45, and 46 are chosen as the main research objects of this paper. The detailed description is in Figure 10.

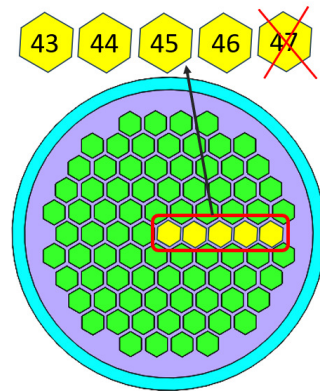


**Figure 10.** Figure of illustration on how to select electrodes for plotting the influence function.

The results were obtained by applying 50 V to each of these four electrodes individually in the finite-element software and then extracting the cross-section data. Figure 11 shows the cross-section lines of the actuator influence function based on the four design options (corresponding to the numbering in Figure 1b). Electrodes No. 43, 44, 45, and 46 are analyzed and numbered from the center region to the boundary regions where the actuator can locally deform when a voltage is applied. The difference in the deformation of each actuator is mainly affected by the electrode position, in which the deformable mirror of the centermost actuator No. 43 has a maximum deformation of 0.399  $\mu\text{m}$  without cutting, and 0.371  $\mu\text{m}$  with a cutting amount of 150  $\mu\text{m}$ , while the deformable mirror of the outermost actuator No. 46 has a deformation of 0.349  $\mu\text{m}$  without cutting within the effective aperture diameter and 0.349  $\mu\text{m}$  without cutting. The maximum deformation of the deformable mirror surface of the outermost actuator No. 46 was 0.349  $\mu\text{m}$  when no cutting was performed in the effective aperture, and the maximum deformation of the deformable mirror surface was 0.326  $\mu\text{m}$  when the cutting amount was 150  $\mu\text{m}$ ; the relationship between the maximum deformation and the number of electrodes is shown in Table 2. As can be seen from Figure 11, the peak value of the influence function curve of each actuator decreases with the increase in the cutting depth. When the cutting depth is the same, the peak value of the influence function is larger and closer to the center position. The cross-linking values of the deformable mirrors reflect the influence of adjacent actuators, which will be analyzed later.

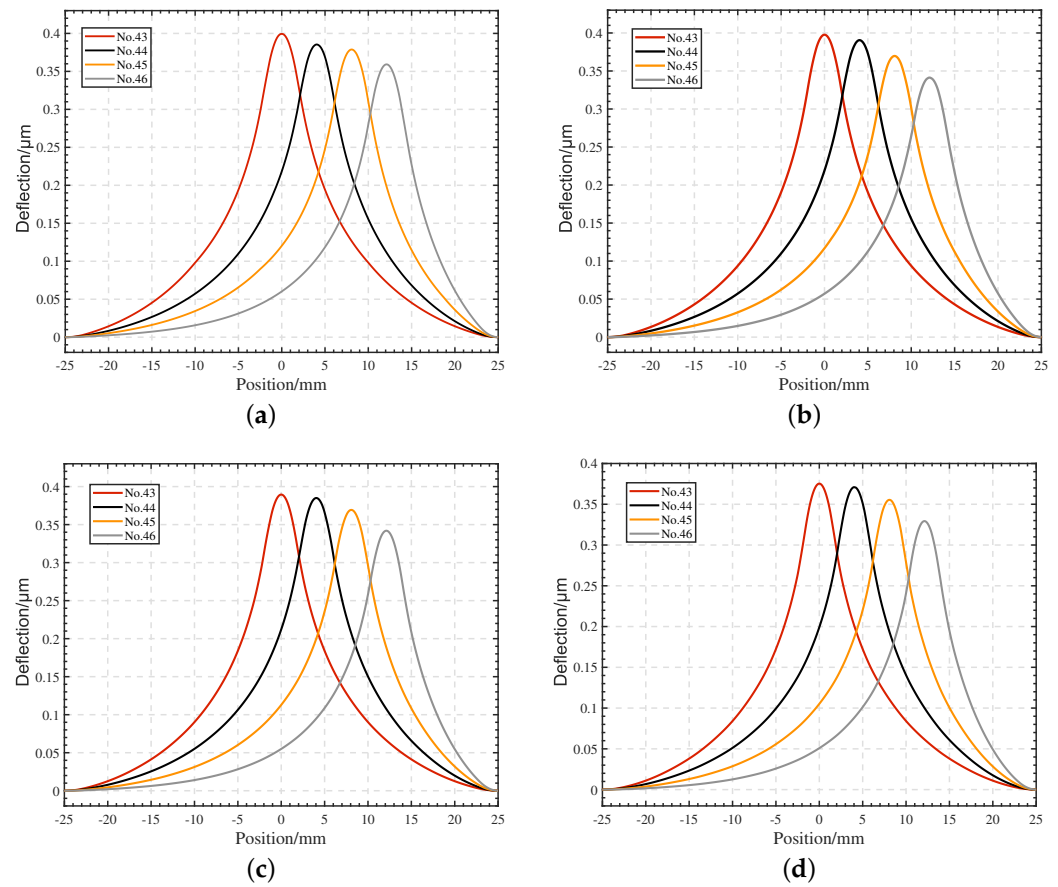


**Figure 11.** Figures of the influence function curves for specific electrodes at different depths of cut: (a) 0  $\mu\text{m}$  depth of cut; (b) 37.5  $\mu\text{m}$  depth of cut; (c) 75  $\mu\text{m}$  depth of cut; (d) 150  $\mu\text{m}$  depth of cut.

**Table 2.** Maximum deformation of electrodes No. 43, 44, 45, and 46 analyzed by influence function curves for four cutting depths.

	0 $\mu\text{m}$	37.5 $\mu\text{m}$	75 $\mu\text{m}$	150 $\mu\text{m}$
No. 43	0.399	0.390	0.383	0.371
No. 44	0.394	0.385	0.379	0.367
No. 45	0.379	0.369	0.363	0.351
No. 46	0.349	0.341	0.336	0.326

The maximum deformation versus the number of electrodes is shown in Table 2, which lists the maximum deformation induced by electrodes No. 43, 44, 45, and 46 at an on-voltage of 50 V when electrode gap cuttings of 0  $\mu\text{m}$ , 37.5  $\mu\text{m}$ , 75  $\mu\text{m}$ , and 150  $\mu\text{m}$  were performed. Taking electrode No. 43 as an example, the maximum deformation shows a decreasing trend when the depth of the cut is gradually increased from 0.399  $\mu\text{m}$ , 0.390  $\mu\text{m}$ , and 0.383  $\mu\text{m}$  to the final 0.371  $\mu\text{m}$ . It can be concluded that the maximum deformation decreases with the increase in the depth of cut.

In this section, the cross-linking values are also calculated and analyzed, and the results are shown in Figure 12. It can be concluded that a deeper cutting depth makes the cross-linking values decrease. This is analyzed with the most minor cutting depth of 150  $\mu\text{m}$ , where the smallest cross-linking value is 35.14% at electrode No. 1. In contrast, the largest cross-linking value is 52.84% at electrode No. 43 (the most central position). An overall trend can also be seen in that, for a certain depth of cut, and the closer the electrode position is to the central region, the greater the cross-linking value.

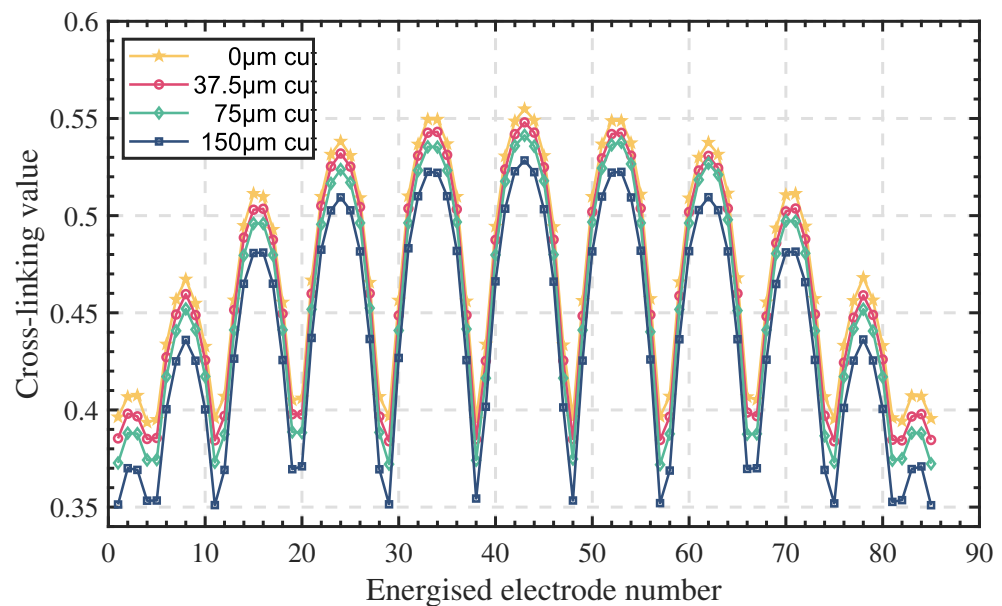


**Figure 12.** Cross-linking value of deformable mirror.

It can be seen in Figure 12 that the general pattern is very similar to Figure 9. The reason is also the same, it is due to the position of the electrode rows that lead to this result. We can see from the figure that cutting only the electrode gap can lead to a significant decrease in the cross-linking value. Therefore, cutting the electrode gap should be considered to achieve the purpose of obtaining the best cross-linking value when designing the deformation mirror when the electrode shape and electrode distribution cannot be changed.

## 5. Conclusions

In this paper, based on 85-unit piezoelectric deformable mirrors, four electrode gap cutting depths were designed. The advantages and disadvantages of different electrode modes were compared, and the effects of the piezoelectric ceramic actuator gap cutting depths on the distribution of the actuator displacement capability and cross-linking values were investigated. The results show that the displacement capability and cross-link value decrease with the increase in the cutting depth and increase with the decrease in the depth. In general, the linear relationship between the input voltage and output deformation is better, and the response is faster when the cross-linking value decreases. Therefore, the cutting piezoelectric deformable mirror can also meet the demand in terms of its compensation ability. The deformable mirror model established by the finite-element method can effectively predict the effect of the cutting depth on the performance of the deformable mirror's electrode gap region and give the magnitude of the actuator displacement and cross-linking value under the simulation conditions, which are guides to the manufacturing process and the use environment of actual piezoelectric deformable mirrors and lay the foundation for the design and manufacture of more-unit deformable mirrors. In the future, we plan to consider deformable mirrors with more electrode shapes, divide the depth level of the cut into more detailed levels, and search for literature to use different cutting methods. Moreover, we will search for a better optical bonding adhesive to adhere piezoelectric materials and mirrors and, subsequently, plan to compensate the piezoelectric hysteresis by control means to further enhance the performance of deformable mirrors.

**Author Contributions:** Conceptualization, B.L. and D.T.; methodology, B.L. and D.T.; software, B.L.; validation, B.L. and D.T.; formal analysis, B.L.; investigation, B.L. and D.T.; resources, B.L. and D.T.; data curation, B.L.; writing—original draft preparation, B.L.; writing—review and editing, B.L. and D.T.; visualization, D.T.; supervision, D.T.; project administration, B.L. and D.T.; funding acquisition, D.T. All authors have read and agreed to the published version of the manuscript.

**Funding:** This research was supported by the CAS Project for Young Scientists in Basic Research (YSBR-066); The Innovation Fund Project of the National Defense Science and Technology of the Chinese Academy of Sciences (CXJJ-21S014); the National Science Foundation of China (T2122001); The Youth Innovation Promotion Association of the Chinese Academy of Sciences (2023230); and Capital construction funds within the budget of Jilin Province (2023C030-6).

**Institutional Review Board Statement:** Not applicable.

**Informed Consent Statement:** Not applicable.

**Data Availability Statement:** The data that support the findings of this study are available from the corresponding author upon reasonable request.

**Acknowledgments:** The authors thank Jian Chen for his supervisory work on this paper. The authors thank the reviewers for their valuable suggestions.

**Conflicts of Interest:** The authors declare no conflict of interest.

## References

1. Nie, G.; Bodda, S.; Sandhu, H.; Han, K.; Gupta, A. Computer-Vision-Based Vibration Tracking Using a Digital Camera: A Sparse-Optical-Flow-Based Target Tracking Method. *Sensors* **2022**, *22*, 6869. [[CrossRef](#)] [[PubMed](#)]
2. Mai, V.; Kim, H. Beaconless angle-of-arrival tracking with improved receiver sensitivity and tracking precision for free-space optical communications. *Opt. Commun.* **2023**, *527*, 128963. [[CrossRef](#)]
3. Hippler, S. Adaptive optics for extremely large telescopes. *J. Astron. Instrum.* **2019**, *8*, 1950001. [[CrossRef](#)]
4. Hardy, J.W. *Adaptive Optics for Astronomical Telescopes*; Oxford Optical and Imaging Sciences: Oxford, UK, 1998; Volume 16.
5. Tyson, R. *Topics in Adaptive Optics*; BoD—Books on Demand: Norderstedt, Germany, 2012.
6. Ellerbroek, B.; Vogel, C. Simulations of closed-loop wavefront reconstruction for multiconjugate adaptive optics on giant telescopes. *Astron. Adapt. Opt. Syst. Appl.* **2003**, *5169*, 206–217.
7. Bifano, T. MEMS deformable mirrors. *Nat. Photonics* **2011**, *5*, 21–23. [[CrossRef](#)]
8. Toporovsky, V.; Kudryashov, A.; Samarkin, V.; Panich, A.; Sokallo, A.; Malykhin, A.; Skrylev, A.; Sheldakova, J. Small-aperture stacked-array deformable mirror made of the piezoceramic combs. In Proceedings of the Laser Resonators, Microresonators, and Beam Control XXIII, Online, 6–12 March 2021; Volume 11672, pp. 183–188.
9. Lukin, V.; Antoshkin, L.; Bolbasova, L.; Botygina, N.; Emaleev, O.; Kanev, F.; Konyaev, P.; Kopylov, E.; Lavrinov, V.; Lavrinova, L.; et al. The history of the development and genesis of works on adaptive optics at the Institute of atmospheric optics. *Atmos. Ocean. Opt.* **2020**, *33*, 85–103. [[CrossRef](#)]
10. Kudryashov, A.; Rukosuev, A.; Nikitin, A.; Galaktionov, I.; Sheldakova, J. Real-time 1.5 kHz adaptive optical system to correct for atmospheric turbulence. *Opt. Express* **2020**, *28*, 37546–37552. [[CrossRef](#)] [[PubMed](#)]
11. Han, X.; Ma, J.; Bao, K.; Cui, Y.; Chu, J. Piezoelectric deformable mirror driven by unimorph actuator arrays on multi-spatial layers. *Opt. Express* **2023**, *31*, 13374–13383. [[CrossRef](#)] [[PubMed](#)]
12. Samarkin, V.; Sheldakova, J.; Toporovsky, V.; Rukosuev, A.; Kudryashov, A. High-spatial resolution stacked-actuator deformable mirror for correction of atmospheric wavefront aberrations. *Appl. Opt.* **2021**, *60*, 6719–6724. [[CrossRef](#)] [[PubMed](#)]
13. Toporovsky, V.; Kudryashov, A.; Samarkin, V.; Rukosuev, A.; Nikitin, A.; Sheldakova, Y.; Otrubyannikova, O. Cooled stacked-actuator deformable mirror for compensation for phase fluctuations in a turbulent atmosphere. *Atmos. Ocean. Opt.* **2020**, *33*, 584–590. [[CrossRef](#)]
14. Hall, S.; Regis, J.; Renteria, A.; Chavez, L.; Delfin, L.; Vargas, S.; Haberman, M.; Espalin, D.; Wicker, R.; Lin, Y. Paste extrusion 3D printing and characterization of lead zirconate titanate piezoelectric ceramics. *Ceram. Int.* **2021**, *47*, 22042–22048. [[CrossRef](#)]
15. Hu, S.; Xu, B.; Zhang, X.; Hou, J.; Wu, J.; Jiang, W. Double-deformable-mirror adaptive optics system for phase compensation. *Appl. Opt.* **2006**, *45*, 2638–2642. [[CrossRef](#)] [[PubMed](#)]
16. Toporovsky, V.; Kudryashov, A.; Skvortsov, A.; Rukosuev, A.; Samarkin, V.; Galaktionov, I. State-of-the-Art Technologies in Piezoelectric Deformable Mirror Design. *Photonics* **2022**, *9*, 321. [[CrossRef](#)]
17. Rousset, G.; Lacombe, F.; Puget, P.; Hubin, N.; Gendron, E.; Fusco, T.; Arsenaault, R.; Charton, J.; Feautrier, P.; Gigan, P.; et al. NAOS—The first AO system of the VLT: On-sky performance. In Proceedings of the Adaptive Optical System Technologies II, Waikoloa, HI, USA, 22–28 August 2002; Volume 4839, pp. 140–149.
18. Xie, L.; Zhong, Z.; Zhang, B. Influence of partially failed actuators of power failure on correction ability of deformable mirrors. *Acta Opt. Sin.* **2021**, *41*, 0223001. [[CrossRef](#)]
19. Furieri, T.; Bonora, S. Large field of view wavefront correction with deformable lenses. In Proceedings of the Free-Space Laser Communications XXXV, San Francisco, CA, USA, 28 January–3 February 2023; Volume 12413, pp. 323–327.
20. Jiang, L.; Hu, L.; Hu, Q.; Xu, X.; Wu, J.; Yu, L.; Huang, Y. Sixty-Nine-Element Voice Coil Deformable Mirror for Visible Light Communication. *Photonics* **2023**, *10*, 322. [[CrossRef](#)]
21. Zhong, G.; Han, X.; Zhang, X.; Lou, J.; Ma, J. Fabrication and Characterization of Deformable Mirror Driven by Piezoelectric Unimorph Actuator Array. *Acta Photonica Sin.* **2022**, *51*, 0151125.

22. Sheldakova, J.; Toporovsky, V.; Galaktionov, I.; Nikitin, A.; Rukosuev, A.; Samarkin, V.; Kudryashov, A. Flat-top beam formation with miniature bimorph deformable mirror. In Proceedings of the Laser Beam Shaping XX, Online, 24 August–4 September 2020; Electr Network, AUG 24-SEP 04, Volume 11486.
23. Galaktionov, I.; Sheldakova, J.; Toporovsky, V.; Kudryashov, A. Numerical analysis of efficiency of light focusing through a moderately scattering medium with the use of deformable mirrors. In Proceedings of the Laser Beam Shaping XXII, San Diego, CA, USA, 21–26 August 2022; Volume 12218.
24. Gowda, H.; Wallrabe, U.; Wapler, M. Higher order wavefront correction and axial scanning in a single fast and compact piezo-driven adaptive lens. *Opt. Express* **2023**, *31*, 23393–23405. [[CrossRef](#)] [[PubMed](#)]
25. Greenwood, D. Bandwidth specification for adaptive optics systems. *J. Opt. Soc. Am.* **1977**, *67*, 390–393. [[CrossRef](#)]

**Disclaimer/Publisher’s Note:** The statements, opinions and data contained in all publications are solely those of the individual author(s) and contributor(s) and not of MDPI and/or the editor(s). MDPI and/or the editor(s) disclaim responsibility for any injury to people or property resulting from any ideas, methods, instructions or products referred to in the content.